Nimodipine fosters remyelination in a mouse model of multiple sclerosis and induces microglia-specific apoptosis

Andrea Schampel[a], Oleg Volovitch[b], Tobias Koeniger[a], Claus-Jürgen Scholz[c,d], Stefanie Jörg[e], Ralf A. Linker[e], Erhard Wischmeyer[f], Marie Wunsch[a], Johannes W. Hell[g], Süleyman Ergün[a], and Stefanie Kuerten[a,1]

[a]Department of Anatomy and Cell Biology, University of Würzburg, 97070 Wuerzburg, Germany; [b]Department of Anatomy and Cell Biology, University of Cologne, 50931 Cologne, Germany; [c]Core Unit Systems Medicine, University Hospital of Würzburg, 97080 Wuerzburg, Germany; [d]The Life & Medical Sciences Institute, University of Bonn, 53113 Bonn, Germany; [e]Department of Neurology, Friedrich-Alexander University Erlangen-Nuremberg, 91054 Erlangen, Germany; [f]Institute of Physiology, Molecular Electrophysiology, University of Würzburg, 97070 Wuerzburg, Germany; and [g]Department of Pharmacology, University of California, Davis, CA 95616

Despite continuous interest in multiple sclerosis (MS) research, there is still a lack of neuroprotective strategies, because the main focus has remained on modulating the immune response. Here we performed in-depth analysis of neurodegeneration in experimental autoimmune encephalomyelitis (EAE) and in in vitro studies regarding the effect of the well-established L-type calcium channel antagonist nimodipine. Nimodipine treatment attenuated clinical EAE and spinal cord degeneration and promoted remyelination. Surprisingly, we observed calcium channel-independent effects on microglia, resulting in apoptosis. These effects were cell-type specific and irrespective of microglia polarization. Apoptosis was accompanied by decreased levels of nitric oxide (NO) and inducible NO synthase (iNOS) in cell culture as well as decreased iNOS and reactive oxygen species levels in EAE. In addition, increased numbers of Olig2$^+$APC$^+$ oligodendrocytes were detected. Overall, nimodipine application seems to generate a favorable environment for regenerative processes and therefore could be a treatment option for MS, because it combines features of immunomodulation with beneficial effects on neuroregeneration.

EAE | microglia | MS | neuroprotection | nimodipine

Multiple sclerosis (MS) is the most prevalent neurological disease of the CNS in young adults and is characterized by inflammation, demyelination, and axonal pathology (1) that result in multiple neurological and cognitive deficits (1–3). Intensive MS research studies have investigated modulating the immune system (4). Common therapeutic strategies are effective in slowing disease progression and attenuating the symptoms, but they cannot cure the disease. The option of preventing neurodegeneration early on would be a valuable addendum to customary treatment (4). Here we suggest that application of nimodipine could be an elegant way to target both neuroinflammation and neurodegeneration. The dihydropyridine nimodipine is commonly known as a 1.2 voltage-gated L-type calcium channel antagonist and is used to treat hypertension and other cardiovascular diseases (5, 6). It also is used to prevent vasospasms after subarachnoidal hemorrhage (5) because of its high affinity for the CNS (7–9). Current research trials are examining its effects on brain injury, epilepsy, cognitive performance, and behavioral effects (6, 7, 10, 11). Its influence on oxidative stress, neuronal survival, synaptic plasticity, and aging also are being investigated, especially within the hippocampus (10, 12). In addition, it was recently shown that the risk of suffering from Parkinson's disease was decreased under treatment with dihydropyridines (13). These studies suggest that nimodipine might have beneficial effects in MS as well, although its role in neurodegenerative diseases that are mediated by inflammatory events has not been well established (6). So far, nimodipine-mediated effects in the CNS have been claimed to result mainly from the modulation of neuronal activity, and studies on the potential effects of nimodipine on (micro)glia have not yet been conducted. Because

immune cell infiltration leads to demyelination and axonal loss by activation of microglial cells, subsequent nitric oxide (NO) release, and oxidative stress (14), we aimed to examine the effects of nimodipine on microglia in more detail in this study. To this end, we used experimental autoimmune encephalomyelitis (EAE) to evaluate the therapeutic impact of nimodipine on MS-like disease in mice (15, 16). Our data demonstrate microglia-specific induction of apoptosis and a decrease in NO and reactive oxygen species (ROS) production, which were accompanied by beneficial effects of nimodipine on remyelination.

Results

Nimodipine Treatment Significantly Attenuated the Clinical Course of EAE. For our studies 96 female 8-wk-old mice on the SJL/J background were immunized with the myelin basic protein (MBP)-proteolipid protein (PLP) fusion protein MP4 in complete Freund's adjuvant (CFA) to induce a relapsing–remitting course of EAE. Immunized mice showed two different clinical EAE phenotypes: 56 mice suffered from the typical form with severe ascending motor deficits, but the other 40 animals showed atypical symptoms, including ataxia and spasticity. Disease onset of typical EAE occurred as early as day 11 after immunization (Fig. 1A), and the onset of atypical EAE (Fig. 1B) was as early as day 12. The clinical data are summarized in SI Appendix, Table S1. Mice were treated

Significance

Multiple sclerosis (MS) is the most frequent neurological disease that leads to premature retirement in young adults. Progressive MS currently is not only incurable, but also untreatable. Here we show that the calcium channel antagonist nimodipine significantly attenuated clinical disease and central nervous system degeneration and also fostered remyelination in a mouse model of MS. The effect of nimodipine was microglia specific, inducing apoptosis and decreasing the production of neurotoxic molecules such as nitric oxide and reactive oxygen species both in vitro and in vivo. These results introduce a treatment option for MS and also may have broad therapeutic implications for chronic neuroinflammatory diseases in general.

Fig. 1. Attenuated clinical course of disease in nimodipine-treated mice. (*A* and *B*) Clinical course of typical (*A*) and atypical (*B*) EAE. All animals were treated on day 23 after immunization with either nimodipine (•; $n = 32$ in the typical EAE group, $n = 18$ in the atypical EAE group) or vehicle solution (□; $n = 24$ in the typical EAE group, $n = 22$ in the atypical EAE group). (*C*) Sensomotor deficits in nimodipine-treated ($n = 10$) and vehicle-treated ($n = 11$) mice were rated using a balance score. *$P \leq 0.05$; ***$P \leq 0.001$ by Mann–Whitney test.

by s.c. injection with either 10 milligrams per kilogram body weight (BW) nimodipine or vehicle (5% EtOH, 5% DMSO, 40% PEG 400, and 50% sterile PBS) for 19–37 consecutive days beginning at day 23 after immunization (the beginning of the first relapse). The dosing regimen was chosen according to the literature (13, 17, 18). The clinical score was significantly attenuated in nimodipine-treated mice in both the typical and atypical EAE groups (Fig. 1 *A* and *B*). We also observed a significant decrease in sensomotor deficits in nimodipine-treated mice compared with vehicle-treated mice (Fig. 1*C*). Furthermore, the relapse rate was significantly higher in vehicle-treated mice than in animals that received nimodipine (*SI Appendix*, Table S2).

Nimodipine Treatment Resulted in Decreased CNS Histopathology and Increased Remyelination. To examine whether the milder course of disease after nimodipine treatment was mirrored by diminished histopathology, ultrastructural analyses of the spinal cord were performed. For that purpose, 12 nimodipine-treated and 9 vehicle-treated mice were killed during chronic EAE (at day 69.60 ± 0.98 for vehicle-treated mice and at day 70.33 ± 0.59 for nimodipine-treated mice) after a treatment duration of 46.60 ± 0.98 d for vehicle-treated mice and 47.33 ± 0.59 d for nimodipine-treated mice. Spinal cords were analyzed via EM. To distinguish between de- and remyelinated nerve fibers, the g-ratio according to Guy et al. (19) was used. This ratio describes the relationship of the myelin sheath to its respective nerve fiber. Analysis of naive mice allowed us to determine the normal range of the g-ratio for each funiculus in each individual segment in the SJL/J spinal cord. In analogy to this ratio we developed the metric we called the "mito-ratio," which describes whether a mitochondrion is enlarged in relation to the axoplasm of its nerve fiber (20). Furthermore, the total number of nerve fibers was calculated to determine axonal loss. Using these parameters, we were able to show that nimodipine-treated animals displayed significantly less neurodegeneration. Treated animals exhibited reduced numbers of demyelinating nerve fibers in both the anterolateral and posterior funiculus compared with their vehicle-treated littermates (Fig. 2*A*). Moreover, the number of nerve fibers showing mitochondrial swelling was decreased (Fig. 2*B*), particularly in the posterior funiculus. In addition, the total number of normal-appearing nerve fibers per square millimeter was increased in nimodipine-treated mice (Fig. 2*C*). Interestingly, the number of remyelinating nerve fibers in both funiculi also was significantly increased after treatment with nimodipine (Fig. 2*D*), suggesting neuroregenerative effects of the drug. Further observation of the oligodendrocyte population demonstrated that the number of Olig2$^+$ cells was significantly elevated in nimodipine-treated mice as compared with vehicle-treated mice and was restored to the level of nonimmunized controls (*SI Appendix*, Fig. S1*A*). In addition, the number of Olig2$^+$APC$^+$ cells was significantly

increased in nimodipine-treated mice (*SI Appendix*, Fig. S1*B*). It was demonstrated that during oligodendroglial regeneration APC is transiently expressed (21). Hence, the increased abundance of Olig2$^+$APC$^+$ cells supports our electron microscopic data showing increased remyelination after nimodipine treatment.

The Extent of Inflammation Did Not Differ Between Nimodipine- and Vehicle-Treated Animals. After studying two of the three hallmarks of MS and EAE—demyelination and axonal pathology—we also investigated inflammation in greater detail. We measured the infiltrate size in seven nimodipine-treated and five vehicle-treated MP4-immunized mice on day 68 or 72 after immunization, respectively (*SI Appendix*, Fig. S2). There were no differences between nimodipine-treated and vehicle-treated animals in either the cellular composition or the size of spinal cord infiltrates. In general, the posterior funiculus was more severely affected than the anterolateral funiculus in both groups, in accordance with the presence of sensomotor deficits in the MP4/SJL model. We also performed flow cytometry for B cells, T cells, T-cell subsets, and T-cell activation on the spinal cord and spleen of five nimodipine-treated and five vehicle-treated MP4-immunized mice during relapse on day 5 after treatment onset (*SI Appendix*, Fig. S3). There was no difference in the T-cell compartment in nimodipine- and vehicle-treated mice. Interestingly, the number of B220$^+$ B cells was increased in the spinal cord but not in the spleen of nimodipine-treated mice. Finally, microarray analyses of the inflammatory response in the spinal cord of MP4-immunized mice confirmed that there was no difference between the two groups at the beginning of the second relapse after a treatment duration of 15 or 20 d, respectively ($n = 3$ mice tested per group) (*SI Appendix*, Fig. S4). A list of all analyzed genes can be found at Gene-Ontology-Terms Class: GO:0006954, inflammatory response. Taken together, our results show that, although the extent of lymphocyte infiltration was unaltered, nimodipine treatment alleviated the clinical signs of MP4-induced EAE.

Nimodipine Treatment Triggered Decreased Cell Viability, Shrinkage, and Apoptosis of Microglial Cells. Although the composition and extent of infiltration were comparable in both groups, we detected differences in the distribution of microglial cells. Nimodipine-treated mice showed a significantly decreased number of Iba1$^+$ cell bodies in both funiculi of the spinal cord on day 29 after immunization compared with vehicle-treated littermates ($n = 4$ in both groups) (Fig. 3 *A* and *B*). Along these lines, we detected significantly more annexin V$^+$ apoptotic cells by flow cytometry in the spinal cord of nimodipine-treated mice ($n = 5$) compared with vehicle-treated mice ($n = 5$) (*SI Appendix*, Fig. S5). Mice were killed on day 29 after immunization after a treatment duration of 5 d. We also stained for TUNEL$^+$Iba1$^+$ microglia in the spinal cord of nimodipine-treated ($n = 5$) and vehicle-treated ($n = 5$)
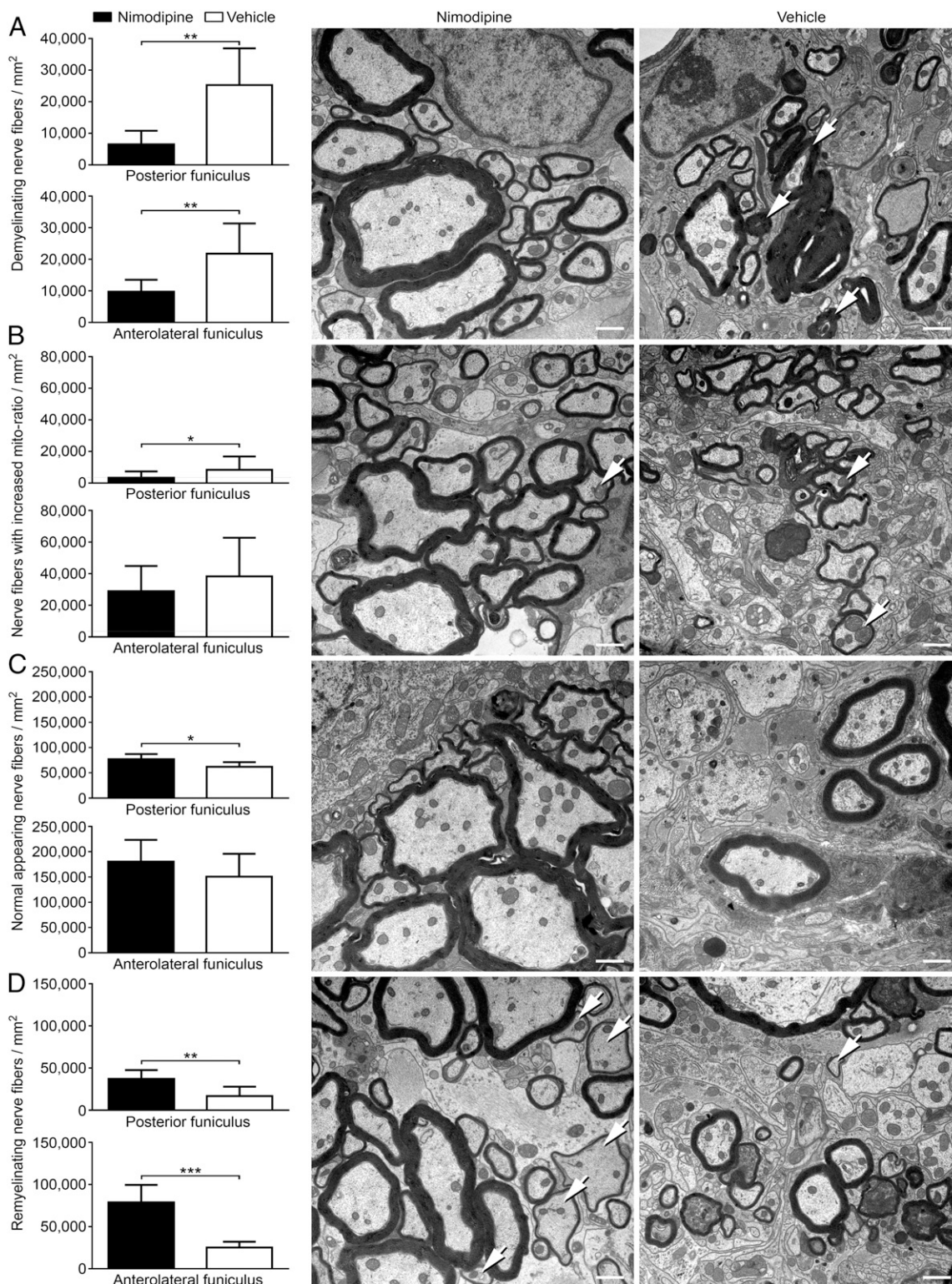
Fig. 2. Decreased nerve fiber pathology and increased remyelination in nimodipine-treated mice. The posterior and anterolateral funiculus of nimodipine-treated (*n* = 12) and vehicle-treated (*n* = 9) mice were analyzed ultrastructurally. For these analyses mice were killed on day 68 or 72, respectively, after immunization. The following parameters were analyzed per square millimeter: demyelinating nerve fibers (*A*), the number of nerve fibers with increased mito-ratio (*B*), axonal loss (*C*), and the number of remyelinating nerve fibers (*D*). (Scale bars: 1 μm.) Arrows indicate representative features of the respective panels. *$P \leq 0.05$; **$P \leq 0.01$; ***$P \leq 0.001$ by two-tailed, unpaired Student's *t* test.

MP4-immunized mice that had received nimodipine or vehicle for 2 d (*n* = 1 mouse per group) or 6 d (*n* = 4 mice per group), respectively, We observed a higher number of double-positive cells in the nimodipine-treated group (*SI Appendix,* Fig. S5). It should be noted, however, that the very low number of double-positive cells in the spinal cord in both groups did not allow statistical

assessment. Interestingly, nonimmunized mice also displayed a reduction of Iba1^{+} cells in the spinal cord following nimodipine treatment. However, this effect was not significant, possibly because of the lower numbers of Iba1^{+} cells in naive animals (*SI Appendix*, Fig. S6). The results were confirmed using organotypic slice cultures of the spinal cord in which treatment with 10 μM

nimodipine for 24 h also led to a significant reduction of Iba1^{+} cells (Fig. 3 *C* and *D*). Inspired by these observations, we studied the effect of nimodipine on microglia in greater detail using two different microglia cell lines (N9 and BV-2). These two cell lines were chosen because their calcium signaling, cytokine production, and cell–cell interactions were reported to be comparable to primary

Fig. 3. Nimodipine treatment leads to shrinkage, rounding, and apoptosis of microglial cells as well as significantly decreased numbers of Iba1^{+} cells in murine spinal cord and organotypic spinal cord culture. (*A*) Number of Iba1^{+} cell bodies/mm^{2} in the spinal cord of animals with EAE. (*B*) Nimodipine treatment (*n* = 4) compared with vehicle-treated mice (*n* = 3). (*C* and *D*). Organotypic slice cultures after treatment with 10 μM nimodipine (*n* = 4) or vehicle (*n* = 3) for 24 h. (*E* and *F*) Number of WGA-stained cells/mm^{2}. (*G*) Viability of N9 cells after treatment with 10 μM nimodipine for 24 h as measured by MTT assay. (*H*) Representative cell-culture images. Arrows indicate cells that display rounding, shrinkage, and pathological vesicles. (*I*) Apoptosis was visualized by TUNEL assay. Arrows indicate positive cells in the respective panels. *$P \leq 0.05$; **$P \leq 0.01$ by two-tailed, unpaired Student's *t* test. Cell-culture data were obtained from at least three independent experiments. (Scale bars: 100 μm.)

cells (22, 23). By applying different doses of nimodipine to N9 and BV-2 cultures for 24 h, we were able to detect a dose-dependent loss of cells. Doses were chosen according to the literature (13, 24, 25). A dose of 1 µM nimodipine did not lead to a significant difference compared with vehicle-treated cells, but in both cell lines a dose of 5 µM significantly reduced the number of microglial cells (Fig. 3 *E* and *F*). The effect was most stable for 10 µM, which was also observed in MTT (3-[4,5-dimethylthiazol-2-yl]-2,5-diphenyltetrazolium bromide) assays (Fig. 3*G*). Results were further confirmed using primary CD11b-sorted cell cultures of adult and newborn murine microglia (*SI Appendix*, Fig. S7). Cells that survived nimodipine treatment frequently showed rounding of the cytoplasm and shrinkage (Fig. 3*H*). Although TUNEL staining was positive in nimodipine-treated microglia cultures after 24 h (Fig. 3*I*), we did not detect apoptosis and cell loss in astrocyte cultures (IMA 2.1 cell line), which were used as glia cell controls (*SI Appendix*, Fig. S8 *A and B*). Likewise, staining of GFAP in the mouse spinal cord and slice culture did not show any evidence for cytotoxic effects of nimodipine on astrocytes (*SI Appendix*, Fig. S8*C*). Therefore the apoptosis-inducing effect of nimodipine seemed to have a certain specificity toward microglia. Furthermore, F4/80+ macrophages in spleen organotypic slice culture were not harmed by nimodipine treatment, indicating specificity even among macrophage populations (*SI Appendix*, Fig. S8*D*). Interestingly, nimodipine-induced apoptosis was independent of microglial polarization toward a proinflammatory (stimulation with TNF-α/IFN-γ) or anti-inflammatory (stimulation with IL-4 or TGF-β1) phenotype (*SI Appendix*, Fig. S9). To test whether the effect was nimodipine specific, we treated N9 cells with different doses of nifedipine, another Ca_v 1.2 dihydropyridine antagonist (*SI Appendix*, Fig. S10 *A and D*); this treatment did not lead to any toxic effects. Because unspecific blockage of potassium channels by high doses of nimodipine could be the reason for microglial apoptosis (26, 27), we applied the potassium channel antagonist 4-AP to N9 cells (*SI Appendix*, Fig. S10 *B and E*). Again, we did not observe any effect on cell viability. The same held true for Bay K8644, a Ca_v 1.2 agonist (*SI Appendix*, Fig. S10*C*). These results were again confirmed in BV-2 cells (*SI Appendix*, Fig. S11).

NO Production and iNOS Expression Are Reduced in Microglia and Murine Spinal Cord After Treatment with Nimodipine. In addition to the effect of nimodipine on microglia apoptosis, we observed reduced NO levels in cell culture after nimodipine treatment of N9 cells using the Griess detection method (Fig. 4*A*). We sought to clarify whether microglia apoptosis alone was the reason for this reduction in NO release. Surprisingly, a similar effect was observed for nifedipine (Fig. 4*B*), which had no effect on cell viability. 4-AP (Fig. 4*C*) and Bay K8644 (Fig. 4*D*) did not have any effect on NO production. Microarray analyses of N9 cells treated with 10 µM nimodipine for 24 h revealed a significantly reduced expression of Nos2 (*SI Appendix*, Fig. S12). Additionally, using immunohistochemistry, we observed reduced levels of iNOS in surviving N9 cells (Fig. 4 *E–F*). Using RT-PCR, we also obtained evidence for decreased iNOS expression in nimodipine-treated EAE mice (Fig. 4*G*). Only 16.7% (one-sixth) of the tested mice treated with nimodipine showed an iNOS mRNA band in the spinal cord, as compared with 60% (three-fifths) of vehicle-treated mice. Because iNOS expression levels were low in EAE lesions, it was impossible to show lesion-specific effects in quantitative RT-PCR (RT-qPCR) analyses of the spinal cord. Instead we chose to investigate ROS, which are strongly produced in EAE lesions, using the dihydroethidium (dHet) detection method (28). The data demonstrate significantly reduced levels of ROS in both funiculi of the spinal cord after treatment with nimodipine (Fig. 4 *H and J*) compared with vehicle-treated animals (Fig. 4 *I and J*). In an attempt to elucidate the mechanism behind the induction of nimodipine-mediated apoptosis, we performed extensive Western blot analyses of iNOS and cleaved poly (ADP ribose) polymerase (cPARP) as a marker for apoptosis (Fig. 4*K*). To this end, N9 cells were incubated with either vehicle or 10 µM nimodipine for 24 h and were continuously observed. Doses of 0.1, 0.5, and 1 µM were tested also, but, in agreement with the other experiments, the effects were

consistently detectable only for 10 µM. We detected a reduction in iNOS protein expression levels after treatment for 24 h and increased levels of cPARP as early as 3 h after treatment onset. After 24 h there was no difference in cPARP expression. Alterations in apoptosis/survival pathways were further determined by microarray analysis. We found significantly decreased Pik3r3 expression in nimodipine- compared with vehicle-treated N9 cells, while mRNA expression of the antiapoptotic factor Bcl2 was significantly increased (*SI Appendix*, Fig. S12) (29). Pik3r3 gene expression is upstream of Akt and a reduction of Akt2 and Akt3 expression levels was likewise detectable in nimodipine-treated N9 cells (*SI Appendix*, Fig. S12).

Nimodipine-Mediated Effects in Microglia Are Independent of Ca_v 1.2 Channel Blockage. Microarray analyses suggested that changes in the apoptosis pathway induced by treatment with 10 µM nimodipine were independent of calcium, because typical Ca^{2+}-modulated gene expression was not significantly altered (*SI Appendix*, Fig. S12). To determine whether the Ca_v 1.2 channel is present in microglial cells, we performed RT-PCR (*SI Appendix*, Fig. S13*A*), RT-qPCR (*SI Appendix*, Fig. S13*B*), and immunohistochemistry (*SI Appendix*, Fig. S13 *C and D*) (30). Although we found Ca_v 1.2 channel expression in the heart, astrocytes, and oligodendrocytes (Oli-neu cells) (*SI Appendix*, Fig. S13 *A–C*), it was absent in microglia, even when stimulated with TNF-α/IFN-γ (*SI Appendix*, Fig. S13*A*). Furthermore, patch-clamp ramp (*SI Appendix*, Fig. S13*E, Upper*) and IV-recordings (*SI Appendix*, Fig. S13*E, Lower*) did not provide convincing evidence for the existence of Ca_v 1.2 in microglia. We performed patch-clamp ramp recordings in the presence of tetraethylammonium (TEA) (*SI Appendix*, Fig. S13*F*) because we wondered whether apoptosis could be induced by unspecific blockage of potassium channels by nimodipine. The measurements displayed a TEA-sensitive outward current with a reversal potential of −76 mV (*SI Appendix*, Fig. S13*F, Upper*). Long-term recording with a holding potential of +30 mV showed the TEA-sensitive fraction of the outward current (*SI Appendix*, Fig. S13*F, Lower*), indicating no or only few scattered potassium channels. It is unlikely that those potassium channels are physiologically relevant, so unspecific blockage of these channels can be ignored as a major cause of apoptosis.

Discussion

Multiple mechanisms contribute to axonal pathology in MS. After initial inflammatory damage, ongoing processes such as dysfunction of mitochondria, generation of free radicals, and oligodendrocyte death lead to demyelination, failure of regeneration, and hence disease progression over time (31). Here we suggest that nimodipine treatment is capable of addressing several of these events. Treatment with nimodipine attenuated the clinical course of MP4-induced EAE, which was mirrored by a decrease in CNS histopathology. While the degree of demyelination and axonal pathology was reduced significantly, the extent of remyelination was significantly increased. Some of these nimodipine-mediated effects are likely to be attributable to calcium channel-dependent events (e.g., in neurons). For instance, we observed decreased mitochondrial pathology in nerve fibers. Furthermore, we detected increased oligodendrocyte survival, which previously was ascribed to the removal of Ca^{2+} but not to a blockade of voltage-gated Na^+ channels (32). However, the astonishing aspect of our study was that nimodipine specifically induced apoptosis in microglia and that this effect was mediated via a mechanism that could not be linked to the blockade of calcium channels, which we expected to be the primary target of nimodipine. The observed effects also could not be linked to unspecific blockage of potassium channels (26, 27, 33, 34). Whether microglia express Ca_v channels is still a matter of debate (35). Our results provide further evidence that they do not. Because it has recently been discovered that microglia mediate neurogenic hypertension and that their depletion leads to significantly attenuated blood pressure (36), the triggering of microglia apoptosis could be an unidentified reason why nimodipine treatment is highly effective

in hypertension. In addition to the apoptosis-inducing effect, we obtained evidence that nimodipine modulates the proinflammatory activity of surviving microglial cells. Along these lines, we found reduced expression levels of Tlr6, Tlr7, and Tlr13, which are known to induce the release of inflammatory cytokines (37). Also, gene-expression levels of carnitine palmitoyltransferase 1A (Cpt1a) and NADPH oxidase 4 (Nox4), were decreased in nimodipine-treated N9 cells (*SI Appendix*, Fig. S12). Most recently Nox4 and Cpt1a expression was linked to the activation of the inflammasome in macrophages (38). Furthermore, inhibition of NADPH oxidase activation in EAE mice was associated with re-duced histopathology, partially via reducing NADPH oxidase-mediated ROS production (28). Indeed, nimodipine treatment decreased the levels of NO, iNOS, and ROS in the CNS. It was shown that excessive NO production and hence peroxynitrite formation occur in MS and EAE lesions, harming oligodendro-cytes and axons (29, 39, 40). In addition, the release of iNOS and NO has been linked to inflammation and neurodegenerative dis-eases in general (40, 41). NO metabolites were even found in the cerebrospinal fluid of MS patients (34), emphasizing the signifi-cance of this pathological mechanism. Current strategies to pro-tect nerve fibers aim at reducing damage by clearing reactive
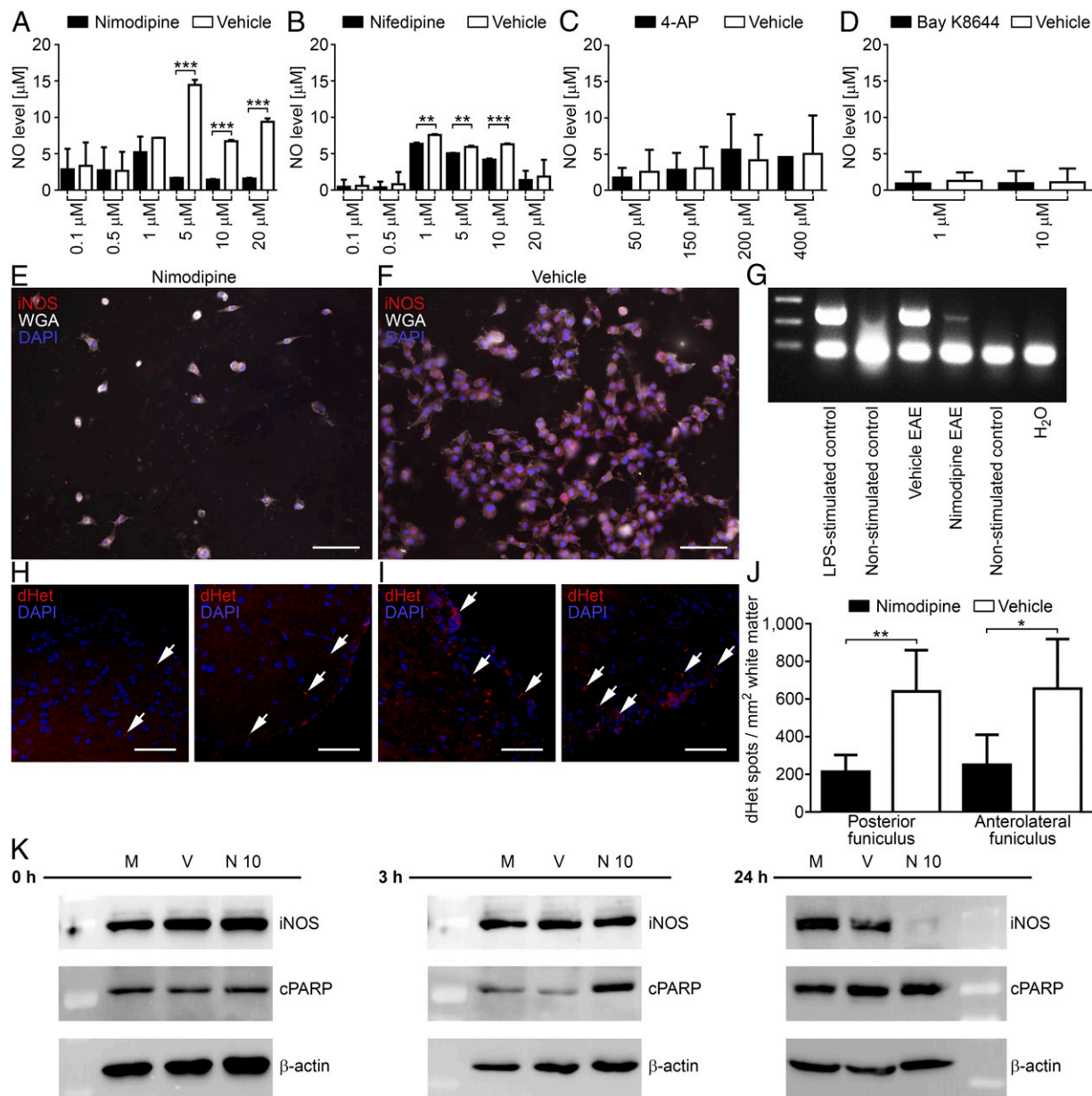
Fig. 4. Decreased NO levels in cell culture and decreased iNOS/ROS levels in spinal cord and cell culture. (*A–D*) NO concentration (stated in micromolars) after N9 cells were treated with different concentrations (stated in micromolars) of nimodipine (*A*), nifedipine (*B*), 4-AP (*C*), and Bay K8644 (*D*) using the Griess detection method. (*E* and *F*) iNOS immunoreactivity in N9 cells after treatment with 10 μM nimodipine (*E*) compared with vehicle (*F*), both counterstained with WGA and DAPI. (*G*) Gene expression of iNOS in nimodipine-treated mice suffering from EAE. (*H* and *I*) ROS production in both funiculi of the spinal cord after treatment with nimodipine (*n* = 5 mice) (*H*) compared with vehicle-treated animals (*n* = 6 mice) (*I*). Images on the left depict the posterior funiculus, and images on the right depict the anterolateral funiculus. Arrows indicate dHet spots. (*J*) Quantification of dHet spots within the white matter per square millimeter showing ROS expression. (*K*) iNOS and cPARP protein expression after nimodipine treatment (10 μM; N10) at three different time points (0, 3, and 24 h after treatment) compared with vehicle treatment (V) and medium control (M). (Scale bars: 100 μm in *E* and *F*; 50 μm in *H* and *J*.) *$P \leq 0.05$; **$P \leq 0.01$; ***$P \leq 0.001$ by two-tailed, unpaired Student's *t* test. Cell-culture data were obtained from at least three independent experiments, each done in triplicate.

oxygen and nitrogen species (42, 43). The blockage of sodium channels also has been reported to attenuate EAE (44). Recently, it was demonstrated that the sodium channel antagonist lamotrigine was effective in protecting axons from exposure to NO (43) and might suppress the activation of innate immune cells, in particular microglia and their migratory activity in MS patients. However, the drug failed in clinical trials because it did not prevent brain atrophy later in disease (42, 45). Nimodipine already has been demonstrated to restore cognitive function (10–12). Combined beneficial effects on neurons and the presumed reduction of toxic neuroinflammation make nimodipine a highly promising candidate for future clinical trials. Another important finding in our study is that nimodipine treatment preserved oligodendrocytes from inflammation-mediated death. Restoring oligodendrocytes by implantation of stem cells is a therapeutic strategy that is currently under consideration (46), but that is certainly more invasive than treatment with a clinically well-known drug such as nimodipine. Taken together, our results show that nimodipine is capable of decreasing the destructive processes in EAE and MS pathology by reducing the number of microglial cells, attenuating inflammation and oxidative stress. Because microglia also have beneficial effects in MS [e.g., the clearance of myelin debris (47)], it is important to note that nimodipine treatment does not deplete all microglia but rather reduces their number and attenuates their production of harmful molecules in the context of ongoing neuroinflammation. Apparently this effect creates a less toxic environment for other cell types, including oligodendrocytes (48), thereby promoting regeneration and still allowing clearance of myelin debris by the remaining microglia (47). Future studies must deal with the transfer of these data into the setting of MS itself. Nimodipine is a well-known cardiovascular drug and typically is used for long-term treatment in patients. Most recently it was shown that patients undergoing long-term antihypertensive therapy with L-type calcium channel blockers had a reduced risk of suffering from Parkinson's disease (13). Because MS patients usually are young and have a robust circulatory system, the long-term application of nimodipine should be safe. However, the feasibility of using nimodipine in daily clinical practice for the treatment of MS will have to be investigated in detail in clinical trials. The potential benefits of developing a combination therapy with one of the existing immune modulatory drugs also should be considered. Overall, our data raise hopes that nimodipine might serve as a treatment option for MS patients that promotes neuroregeneration while also having immunomodulatory capacity in the absence of severe side effects.

Materials and Methods

Mice. Female SJL/J mice (6–8 wk old, $n = 104$) were obtained from Janvier or Harlan and were maintained under specific pathogen-free conditions in the animal facilities of the Department of Anatomy, University of Cologne or the Department for Functional Materials in Medicine and Dentistry (FMZ), University of Würzburg. Because mice were obtained from different vendors, only those that showed comparable clinical courses were included in this study. All animals had free access to standard rodent diet (Altromin; catalog no. 1314) and autoclaved tap water. Room temperature was kept between 20–22 °C at 65% humidity. Twelve-hour light/dark periods were ensured. Animals suffering from EAE were granted easier access to water and food. All animal experiments complied with the German Law on the Protection of Animals, the principles of laboratory animal care set forth in NIH publication No. 86–23, revised 1985 (49), and the ARRIVE (Reporting Animal Research of in Vivo Experiments) guidelines. The treatments were performed according to a protocol approved by the Landesamt für Natur, Umwelt und Verbraucherschutz Nordrhein-Westfalen (LANUV) and the Regierung von Unterfranken, Germany (approval numbers 84-02.04.2012.A269 and 55.2-2531.01-118/13).

EAE Induction and Drug Treatment. Female 8-wk-old mice ($n = 96$) were immunized s.c. into both sides of the flank with the myelin basic protein (MBP)–proteolipid protein (PLP) fusion protein MP4. Each mouse received 200 µg MP4 emulsified in CFA, which consisted of a 9:1 mixture of paraffin oil (Sigma; catalog no. 18512) and mannide monooleate (Sigma; catalog no. M8819) and contained *Mycobacterium tuberculosis* strain H37 Ra (BD Biosciences; catalog

no. 231141) at a concentration of 5 mg/mL. MP4 was obtained from Alexion Pharmaceuticals Inc. Mice were scored daily for the occurrence of signs of EAE. For mice suffering from typical EAE, the standard EAE scoring system was used: no EAE, 0; beginning tail paresis, 0.5; tail paresis, 1; hind limb weakness, 2; beginning hind limb paresis, 2.5; complete hind-limb paresis, 3; quadriplegia, 4; and death, 5. For atypical EAE, a balance score was used to rate sensomotor deficits that occurred mainly in the atypical form. Mice were encouraged to balance over a distance of 10 cm on a metal bar and were rated according to following parameters: no problems balancing, 0; not able to balance over the whole distance but able to stay on the bar, 1; and falling off the bar, 2. In addition, to compare the disease course in the typical and atypical groups, the standard EAE score also was used to grade atypical EAE but was modified to account for the frequently absent tail paresis (*SI Appendix*, Fig. S14). Nimodipine or vehicle was applied by daily s.c. injections starting on day 23 after immunization. Mice were injected with either 10 mg/kg BW nimodipine (Bayer HealthCare AG) in vehicle solution, which consisted of 5% ethanol, 5% DMSO (Sigma; catalog no. D8418), 40% PEG 400 (Sigma; catalog no. 202398), and PBS or were treated with vehicle solution only. Because nimodipine is very light sensitive, all steps, including stock preparation and administration, were performed protected from light. Nonimmunized animals ($n = 8$) were treated for 10 d. In all treatment cohorts, mice were matched before treatment onset so that the mean score was not significantly different between groups. If one treatment group was slightly more affected by EAE, we chose this group for nimodipine treatment so that a potential treatment effect was more profound. To ensure that the doses of nimodipine used both in vivo and in vitro in our study were clinically relevant, we followed the recommendations in published studies (6, 13, 18, 50, 51). All doses described in the quoted literature were able to attenuate cognitive deficits in models of neurodegenerative diseases and to trigger endogenous hormone responses, so it is likely that sufficient levels of the drug were achieved in the CNS (13, 50, 52). Furthermore, many studies on subarachnoidal hemorrhage have shown that the dosages used in animal studies are able to induce comparable effects in patients (51, 52).

Tissue Preparation. Mice were deeply anesthetized with CO_2 and were perfused intracardially with 4% paraformaldehyde (PFA) in PBS (pH = 7.4) for ROS detection and immunohistochemistry or with 4% PFA and 4% glutaraldehyde (GLA) in PBS (pH = 7.4) for EM. The spinal cord was postfixed in perfusion solution at 4 °C for 24 h and was removed carefully from the vertebral canal. The lumbar part of the spinal cord was divided into three equidistant segments that were embedded in EPON liquid epoxy resin (Hexion) for EM or in paraffin for immunohistochemistry. For ROS detection the spinal cord was cryoprotected in 10% sucrose at 4 °C for 2–3 h, followed by 30% sucrose at 4 °C overnight. Afterwards, spinal cord sections were stored in TissueTek (Tissue Tek O.C.T. Compound; Sakura; catalog no. 4583) and subsequently were snap-frozen in isopentane and liquid nitrogen.

Semithin Sectioning and EM. Spinal cord tissue was fixed overnight in 4% PFA/4% GLA after perfusion and was removed carefully from the vertebral canal. The lumbar part was separated and split into three segments as described above. These segments were embedded in EPON. For this purpose several steps were taken. To get rid of the abundant fixative, spinal cord segments were washed with 0.1 M cacodylate (CACO) buffer (pH 7.35) three times on a rotating wheel for 30 min each. Afterwards the tissue was placed into 0.1 M CACO buffer containing 2% osmium tetroxide at room temperature for 3 h. During that time the tissue was protected from light and was deposited on a rotator. The tissue then was washed again three times (30 min each) with 0.1 M CACO buffer. The next day the tissue was transferred into 90% ethanol at room temperature for 30 min and subsequently was washed three times in 100% ethanol (30 min each). The tissue then was transferred into a 1:1 mixture of propylene oxide and ethanol for 30 min at room temperature and afterwards was treated with pure propylene oxide for 30 min before embedding in EPON. Embedded tissue was cut transversely at 500 nm with an ultra-microtome (Ultracut UCT; Leica) for semithin analysis. Sections were rinsed in methylene blue for ~1.5 min. Sections were dried on a heating plate and covered with Entellan (Merck). Digital images were acquired using a Leica DM LB2 microscope equipped with a Zeiss camera (AxioCam MRc) and Zeiss software (AxioVision 40 4.7). Image-Pro Plus software 6.0 (Media Cybernetics, Inc.) was used to analyze six to eight images of two lumbar spinal cord sections per mouse, covering both funiculi completely. For EM analysis tissue was cut into 80-nm-thick sections. Sections were stretched with xylene while floating in the water tub of the diamond knife. Afterwards they were placed carefully on 150-mesh hexagonal formvar-coated copper grids (Electron Microscopy Sciences). For contrast enhancement the sections were stained with 1% aqueous uranyl acetate solution for 20 min and with Reynold's lead citrate solution for 7 min. The total areas within the anterolateral funiculus and the posterior funiculus were analyzed separately

using a Zeiss 902A transmission electron microscope at 80 kV acceleration voltage. Digital pictures were taken with an EM digital camera system (MegaView, analysis document 3.2; Olympus Soft Imaging Systems GmbH) at magnifications of 3,000× and 7,000×.

Immunohistochemistry. Murine spinal cords were deparaffinized and boiled for 10 min in 10 mM citrate buffer (pH 6) for antigen retrieval. Sections were washed with PBS, blocked with 1% normal goat serum (NGS) in PBS at room temperature for 1 h, followed by incubation with the primary antibody (anti-Iba1; Wako Laboratories; catalog no. 019-19741) diluted 1:1,000 in PBS or anti-GFAP (Sigma; catalog no. G 3893) diluted 1:500 in blocking solution at 4 °C overnight. Subsequently, the sections were washed three times in PBS and were incubated with the secondary antibody, Cy3-conjugated goat anti-rabbit IgG (Jackson ImmunoResearch; catalog no. 111-165-003) for Iba1 or Cy3-conjugated goat anti-mouse IgG (Jackson ImmunoResearch; catalog no115-165-003) for GFAP, each diluted 1:600 in PBS at room temperature for 1–2 h. After renewed washing, sections were counterstained with DAPI (1:1,000) (Roche; catalog no. 236276), washed, and coverslipped with n-propyl gallate (NPG) (Fluka; catalog no. 48710). For Iba1/TUNEL staining the same protocol was used, but after antigen retrieval the sections were stained for TUNEL using the ApopTag Red In Situ Apoptosis Detection Kit (Millipore; catalog no. S7165) according to the manufacturer's instructions. Immunofluorescent images were acquired using a Keyence BZ-9000 fluorescence microscope. For light microscopic staining of Olig2, spinal cord sections were blocked with 3% hydrogen peroxide in distilled water at room temperature for 10 min. Subsequently, sections were permeabilized with 0.25% Triton-X in PBS for 10 min, followed by blocking with 5% NGS in PBS at room temperature for 1 h. Next, sections were incubated with anti-Olig2 (Merck Millipore; catalog no. Ab 9610) diluted 1:500 in 1% NGS in PBS at room temperature for 1 h, followed by incubation with the secondary antibody, biotinylated goat anti-rabbit IgG (Vector Laboratories; catalog no. BA-1006) diluted 1:250 in 1% NGS in PBS at room temperature for 30 min. Next, sections were incubated for 30 min with the ABC kit (Vectastain Elite; Vector Laboratories; catalog no. PK-6100 Standard) according to the manufacturer's instructions, followed by development with the DAB (3,3′-diaminobenzidine-tetrahydrochloride) peroxidase substrate kit (Vector Laboratories; catalog no. SK-4100), according to the manufacturer's instructions, at room temperature for ~15 min. Sections were counterstained with hematoxylin for 10 min and were coverslipped with Aqua Poly/Mount (Polysciences; catalog no. 18606). For fluorescence staining of Olig2 and APC, the same protocol was used, but the primary antibody was incubated overnight at 4 °C. Subsequently, the sections were incubated with the secondary antibody, Cy5-conjugated goat anti-rabbit IgG (Jackson ImmunoResearch; catalog no. 111-175-144) diluted 1:250 in PBS together with DAPI (1:5,000; Roche; catalog no. 236276) at room temperature for 30 min. For double staining with anti-APC antibody, the sections were again blocked with 5% NGS in PBS at room temperature for 1 h. The anti-APC antibody (Calbiochem; catalog no. OP80) was diluted 1:100 in 1% NGS in PBS and applied at room temperature for 2 h. Subsequently, sections were incubated with the secondary antibody, biotinylated goat anti-mouse IgG (Vector Laboratories; catalog no. BA-9200) diluted 1:250 in 1% NGS in PBS and applied at room temperature for 30 min. Afterwards the sections were incubated with NeutrAvidin DyLight 550 (Thermo Scientific; catalog no. 84606) at room temperature for 30 min. Sections were coverslipped with Mowiol 4-88 (Roth; catalog no. 0713.1). The number of positive cell bodies per square millimeter of the respective funiculus was counted. For this purpose six to eight images of three segments of the spinal cord per mouse, covering both funiculi completely, were analyzed. The depicted area was measured using Image-Pro Plus software 6.0 (Media Cybernetics, Inc.).

Immunocytochemistry. Microglial cells were seeded at 250,000 cells/mm^2 on rounded coverslips (diameter: 12 mm) that had been mounted with 0.001% poly-ornithine/dH$_2$O (Sigma; catalog no. P4957) 2 h previously. They were allowed to settle for 24 h in the incubator (37 °C, 3.5% CO$_2$) and were treated for an additional 24 h with 10 μM nimodipine or vehicle. Subsequently, they were fixed with 2% PFA at 4 °C for 2 h. Cells were washed with PBS, blocked with 3% BSA/1% NGS in PBS, and incubated with anti-iNOS antibody (BD Biosciences; catalog no. 610432) diluted 1:150 in blocking solution at 4 °C overnight. Subsequently, sections were washed with PBS and incubated with the secondary antibody, Cy3-conjugated goat anti-rat IgG (Jackson ImmunoResearch; catalog no. 112-165-003), diluted 1:500 in blocking solution. After renewed washing, sections were counterstained with Texas Red-X–conjugated wheat germ agglutinin (WGA) (Invitrogen; catalog no. W21405), diluted 1:200 in PBS, and DAPI, diluted 1:2,000 in PBS, and were coverslipped with Mowiol 4-88 (Roth; catalog no. 0713.1). For the detection of the Ca$_v$ 1.2 channel, the same protocol was used. Because the antibody (diluted 1:400 in blocking solution) (Alomone Labs; catalog no. ACC-003-AG) was directly conjugated with ATTO-488, no secondary

antibody was needed. Goat anti-rabbit FITC-conjugated IgG (Jackson Immuno-Research; catalog no. 111-095-003) was used as background control. Immunofluorescent images were acquired using a Keyence BZ-9000 fluorescence microscope. Confocal laser-scanning microscopy images were taken using a Nikon A1R+ confocal microscope system equipped with an Eclipse TI-E inverse microscope with coherent sapphire lasers and a visible fiber laser (lines: 405, 488, 561, 647 nm) (MBP Communications). Plan-Apochromat 20× NA 0.8, Plan-Apochromat 60× NA 1.4, and Apochromat 100× NA 1.5 objectives were used for detection in three simultaneous channels. The system was equipped with NIS-Elements Advanced Research Software (Nikon). ImageJ (1.47v; NIH) was used for editing of confocal laser-scanning microscope images.

ROS Detection. Mice treated with either 10 mg/kg BW nimodipine or vehicle and untreated immunized and nonimmunized controls were s.c. injected with dHet (Molecular Probes by Life Technologies; catalog no. D11347) and were killed 3 h later to evaluate the amount of ROS in the spinal cord. Afterwards, mice were intracardially perfused with PBS, followed by 4% PFA in PBS. Spinal cords were removed and postfixed in 4% PFA at 4 °C for 24 h. Subsequently, the tissue was washed with PBS, stored in 10% sucrose at 4 °C for 2–3 h, and incubated overnight in 30% sucrose. The tissue was placed into TissueTek and snap-frozen in isopentane and liquid nitrogen. The spinal cord was transversally cut with a Leica cryostat into 10-μm-thick sections for fluorescence microscopic analyses and into 30-μm-thick sections for confocal analyses and were counterstained with DAPI (1:2,000 in PBS). The protocol was adapted from Choi et al. (28).

RNA Extraction, RT-PCR, and Microarray Analysis. Total RNA was isolated from homogenized murine tissue or murine N9 cell pellets by the use of TRIzol (Invitrogen Life Technologies; catalog no. 15596018) for 5 min. Afterwards chloroform was added to the lysate, which was centrifuged at 13,000 × g at 4 °C for 15 min. The supernatant was precipitated by isopropanol at room temperature for 10 min. Subsequently, ethanol was added to the RNA pellet, mixed well, and centrifuged at 7,500 × g and 4 °C for 5 min. The pellet was dried and resuspended in diethylpyrocarbonate (DEPC) water, stored at −80 °C for at least 1 h, and quantified. The concentration of each RNA extract was determined by spectrophotometric measurement using a Nanodrop 2000c spectrophotometer (Thermo Fisher Scientific). The RNA was reversely transcribed using the Qiagen QuantiTect reverse transcription kit (Qiagen; catalog no. 205313) according to the vendor's instructions. cDNA was used as a template for RT-PCR and RT-qPCR. The RT-PCR mixture for a reaction consisted of 9.5 μL MgCl$_2$ (50 mM), 0.75 μL of each primer (concentration: 10 μM), 12.5 μL Red Taq Mix (Genaxxon Bioscience; catalog no. M3029), and 1 μL template. RT-PCR was performed in a thermal cycler (Applied Biosystems; catalog no. 2720) using a total reaction volume of 25 μL. Thermocycling conditions were 95 °C for 5 min, followed by 35 cycles of 95 °C for 30 s, 58 or 60 °C, respectively, for 30 s, and 72 °C for 30 s (*SI Appendix*, Table S3). Amplified products were separated on an 1% agarose gel in 1× Tris/acetate/EDTA buffer (pH 8.0) containing 0.005% Midori Green (Biozym; catalog no. 617004). RT-PCR products were visualized under UV light. The housekeeping gene *GAPDH* was used as a loading control. RT-qPCR was performed in 0.1-mL PCR vials (Qiagen) in the Qiagen Rotor Q (Qiagen). Each 20-μL reaction contained 10 μL of Qiagen Master Mix (QuantiNova SYBR Green Master PCR Kit; Qiagen; catalog no. 208052), gene-specific forward and reverse primer mix (final concentration of 1 μM each), RNase-free water, and ~200 ng of cDNA per reaction. No-template controls contained nuclease-free water instead. The cycling conditions were 95 °C for 2 min to activate the DNA polymerase followed by 35 cycles at 95 °C for 20 s for denaturation, 20 s of annealing at 60 °C, and 20 s of elongation at 72 °C. At the end of the amplification cycles, melting curves were used to validate RT-qPCR product specificity. All RT-qPCR runs included a no-template negative control for each primer set. All samples were amplified in triplicate. Data were analyzed using the ΔΔ cycle threshold (Ct) method (30). Expression levels were normalized to the Ca$_v$ 1.2 gene-expression level of IMA 2.1 cells. The relative expression of our gene of interest was defined as the ratio of the expression of the gene in diverse cell types to that in IMA 2.1 cells. GAPDH was used as a control in establishment experiments. Primers were provided by biomers.net GmbH and Eurofins Genomics and are listed in *SI Appendix*, Table S3. For microarray analyses total RNA was isolated from murine spinal cord tissue or N9 cell pellets using the TRIzol method as described above. Before sample preprocessing, RNA integrity was assessed with the RNA 6000 Nano Kit (Agilent) using the Bioanalyzer 2100 instrument (Agilent). One hundred nanograms of each sample were processed with the whole-transcript WT PLUS Kit (Affymetrix), i.e., subjected to RNA amplification via reverse transcription to double-stranded cDNA and subsequent in vitro transcription; this processing was followed by another round of reverse transcription yielding single-stranded DNA in sense orientation. Hybridization mixtures were produced

after fragmentation and biotin labeling of target DNAs. Microarray hybridization to GeneChip Mouse Gene 2.0 ST arrays (Affymetrix) was performed according to the manufacturer's protocol using the Fluidics Station 450 with the program FS450_0002. Background correction, normalization, and gene-level probeset summary were performed using the Expression Console v1.2.1.20 (Affymetrix). Differentially expressed genes were determined for nimodipine- vs. vehicle-treated samples with the false-discovery rate of differential expression being estimated with an empirical Bayes methodology using a lognormal/normal data modeling (53). Microarray data were deposited at Gene Expression Omnibus (GEO) (https://www.ncbi.nlm.nih.gov/geo) in entry GSE87397.

Cell Culture. N9, BV-2, and IMA 2.1 cell lines were grown in DMEM (Gibco by Thermo Fisher Scientific; catalog no. 41966) containing 10% FBS (Gibco by Thermo Fisher Scientific; catalog no. 10270), penicillin (100 IU/mL penicillin G sodium salt) (Sigma; catalog no. P3032), and streptomycin (100 mg/mL streptomycin sulfate salt) (Sigma; catalog no. S6501) and were maintained at 37 °C and 3.5% CO_2. Nimodipine diluted in vehicle solution (consisting of DMSO, ethanol, and PEG-400, analogous to treatment in mice) or vehicle solution alone was added to the medium and applied for 24 h. Several final concentrations (1, 5, 10, and 20 µM) were tested. The final concentration of DMSO and ethanol was below the proapoptotic range. Proapoptotic effects of DMSO or ethanol alone were also excluded by performing corresponding vehicle-control experiments. To ensure that our in vitro dose of nimodipine is clinically relevant, we studied the literature closely and tested doses that already had been used in several CNS disease models (13, 18, 50, 51). The dose used for cell culture had been shown to induce equivalent effects in patients (e.g., reduced stress-mediated effects after brain surgery and decreased excitotoxicity) (51). Stimulation was performed with 100 ng/mL TNF-α (PeproTech; catalog no. 315-01A), IFN-γ (PeproTech; catalog no. 345-05), 100 ng/nL TGF-β1 (PeproTech; catalog no. 100-21), or 10 ng/mL IL-4 (PeproTech; catalog no. 214-14). MTT (Vybrant MTT cell proliferation assay kit, quick protocol; Molecular Probes; catalog no. V-13154) was used to determine cell viability. The absorbance was measured at 540 nm using a Victor³ ELISA reader (Victor3 1420 Multilabel counter, software version 3.00, revision 5; Perkin-Elmer). Apoptosis was visualized by TUNEL assay (DeadEnd fluorometric TUNEL system; Promega; catalog no. G3250). For nitrite quantification the Griess assay (Molecular Probes by Thermo Fisher Scientific; catalog no. G-7921) was used. Absorbance was measured at 548 nm using a Victor³ ELISA reader (Perkin-Elmer). For this purpose cells were cultured in phenol-free DMEM (Gibco by Thermo Fisher Scientific; catalog no. 31053).

Microglia Isolation and Cultivation. Microglia cells were isolated from adult mouse brain using the Adult Brain Dissociation Kit (Miltenyi Biotec; catalog no. 130-107-677) or from newborn mice using the Neural Tissue Dissociation Kit T (Miltenyi Biotec; catalog no. 130-093-231). Briefly, adult brains were removed, washed in Dulbecco's phosphate-buffered saline (DPBS) (Sigma Aldrich; catalog no. D8662), and cut into sagittal slices. The tissue was dissociated by enzymatic digestion on a gentleMACS Octo Dissociator (Miltenyi Biotec; catalog no. 130-095-937). The cell suspension was filtered through a 70-µM cell strainer (Miltenyi Biotec; catalog no. 130-095-823) and was washed with cold DPBS before debris and red blood cells were removed. The cells then were labeled with CD11b MicroBeads (Miltenyi Biotec; catalog no. 130-093-634) for 15 min, washed, and processed by magnetic separation on LS columns (Miltenyi Biotec; catalog no. 130-042-401). CD11b magnetically labeled cells were flushed out by pushing the plunger into the column. The magnetic separation was repeated to increase the purity of microglia cells. Cells were resuspended in DMEM containing 10% horse serum (Sigma; catalog no. H1138) and 1% penicillin/streptomycin (Pan Biotech; catalog no. P06-07100) and were seeded at a density of 1×10^5 cells per well on poly-D-lysine–precoated culture plates (0.002%) (Sigma; catalog no. P0899) for 3 h at 37 °C. Microglia from newborns were isolated with the Neural Tissue Dissociation Kit T according to the manufacturer's instructions and were seeded on poly-D-lysine–precoated culture plates for 14 d in DMEM (Gibco; catalog no. 41966-029) containing 10% horse serum (Sigma; catalog no. H1138) and 1% penicillin/streptomycin (Pan Biotech; catalog no. P06-07100), hereafter called "MGC medium." Culture medium was changed every 2 to 3 d. Microglia cells were purified by using CD11b MicroBeads and magnetic separation on LS columns as described before. Purified cells were resuspended in MGC medium and seeded at a density of 50,000 cells per well on poly-D-lysine–precoated culture plates for 3 h at 37 °C.

Flow Cytometry. Single-cell suspensions were analyzed by staining for extra- and intracellular markers. Dead cells were excluded by a fixable viability dye, eFluor780 (eBioscience; catalog no. 65-0865-14), and Fc block was performed using αCD16/32 (eBioscience; catalog no. 16-0161). For intracellular cytokine staining, cells were stimulated for 4 h with ionomycin (1 µM) (Sigma; catalog

no. I3909) and phorbol-12-myristate-13-acetate (PMA) (50 ng/mL) (Sigma; catalog no. P1585) in the presence of monensin (2 µM) (eBioscience; catalog no. 00-4505-51). Cells were stained for surface markers with the respective fluorochrome-conjugated antibodies for 30 min and were permeabilized using Fix/Perm (eBioscience catalog; no. 00-5523-00) according to the manufacturer's protocol. Intracellular cytokines were stained with the respective fluorochrome-conjugated antibodies for 30–45 min. Cells were analyzed with the FACSCanto II flow cytometer and FACSDiva software (BD Bioscience). Data analysis was performed with FlowJo (TreeStar). Apoptosis was analyzed by incubating the cells in 500 µL annexin V binding buffer (BD Pharmingen; catalog no. 556454) containing 5 µL annexin V FITC (BD Pharmingen; catalog no. 556419) and 5 µL propidium iodide (BD Pharmingen; catalog no. 51-66211). After 15-min incubation, cells were washed and analyzed with the BD FACSCanto II. The following fluorochrome-conjugated anti-mouse antibodies were used: CD4-FITC (RM4-5; eBioscience; catalog no. 11-0042-8), CD8a-BV510 (53-6.7; BioLegend; catalog no. 100752), CD11b-PE (M1/70; BioLegend; catalog no. 101207), CD25-PeCy5 (PC61; BioLegend; catalog no. 102010), CD44-PE (IM7; BioLegend; catalog no. 103008), CD45-V450 (30-F11; eBioscience; catalog no. 560501), CD45R/B220-BV510 (RA3-6B2; BioLegend; catalog no. 103247), CD62L-APC (MEL-14; eBioscience; catalog no. 17-0621-83), FoxP3-PE (FJK-16s; eBioscience; catalog no. 12-5773-82), IFN-γ-APC (XMG1.2; eBioscience; catalog no. 17-7311-82), and IL-17A-PE (eBio17B7; eBioscience; catalog no. 12-7177-81).

Patch Clamp. N9 cells were seeded on rounded coverslips (10-mm diameter) and allowed to settle in the incubator (37 °C, 3.5% CO_2) for 24 h. Subsequently, cell recordings were performed at room temperature in a bath solution consisting of 140 mM tetraethylammonium chloride, 2 mM $MgCl_2$, 20 mM $BaCl_2$, 10 mM glucose, and 10 mM Hepes, pH 7.4. Patch pipettes were pulled from borosilicate glass capillaries (Science Products) and sharpened to give input resistances of 2–4 MΩ. The pipette recording solution contained 100 mM CsCl, 20 mM tetraethylammonium chloride, 1 mM $MgCl_2$, 5 mM MgATP, 10 mM Hepes, and 10 mM EGTA (pH 7.3). The bath solution for recordings of potassium channels consisted of 135 mM NaCl, 5.4 mM KCl, 1.8 mM $CaCl_2$, 1 mM $MgCl_2$, 10 mM glucose, and 5 mM Hepes, pH 7.4. The pipette recording solution contained 140 mM KCl, 0.01 mM $CaCl_2$, 2 mM $MgCl_2$, 1 mM EGTA, 1 mM Na_2ATP, 0.1 mM cAMP, 0.1 mM GTP, and 5 mM Hepes, pH 7.3. Currents were recorded with an EPC-9 patch-clamp amplifier (HEKA) and were low-pass filtered at 2.9 kHz. Data analysis was performed with Igor Pro (WaveMetrics). Leak currents were digitally subtracted. Steady-state current voltage relations were obtained by applying voltage ramps between +60 and −150 mV. Cell resistance was measured continuously during the experiments.

Immunoblotting. Total protein lysates were obtained from N9 cells by lysing the samples in cold radioimmunoprecipitation assay (RIPA) buffer in the presence of PMSF (Sigma; catalog no. 78830-5G) and the protease inhibitors aprotinin (AppliChem; catalog no. A2131), pepstatin A (AppliChem; catalog no. A2205), leupeptin hemisulfate (AppliChem; catalog no. A2183), sodium fluoride (Merck; catalog no. 6649), and sodium orthovanadate (Sigma; catalog no. s6508). Protein concentration was evaluated by BCA assay (Pierce BCA Protein Assay Kit; Thermo Fisher Scientific; catalog no. 23225). Western blot analyses were performed with antibodies against iNOS (1:500) (BD Biosciences; catalog no. 610432), cPARP (1:1,000) (Cell Signaling; catalog no. Asp214), and β-actin (1:1,000) (Sigma; catalog no. A1978) diluted in blocking solution: 1× TBS + 0.25% Tween 20 (AppliChem; catalog no. A1389) (TBST) buffer containing 5% milk. All secondary antibodies were conjugated with HRP and diluted at 1:1,000 in blocking solution (goat anti-rabbit IgG for cPARP (Jackson ImmunoResearch; catalog no. 111-035-003), goat anti-mouse IgG for iNOS, and β-actin (Jackson ImmunoResearch; catalog no. 115-035-068). ECL Prime Western blotting detection substrate (Amersham; catalog no. RPN2232) was used for the detection of HRP on immunoblots with a digital imaging system (Vilber Lourmat; Fusion Solo VL-35.F0.84).

Slice Culture and Staining. For slice culturing mice were killed by cervical dislocation, and the lumbar section of the spinal cord was quickly removed and stored on ice. Subsequently, the tissue was embedded in 2% agarose in PBS and was sectioned into transverse slices (200 µm) using a vibratome (Leica VT 1000S, Leica), stored in cold PBS containing 2% penicillin/streptomycin, and subsequently cultured in DMEM containing 10% FBS, penicillin (100 IU/mL), and streptomycin (100 mg/mL) at 37 °C and 3.5% CO_2. Drug treatment was performed as in the cell-culture experiments and was applied for 24 h. For immunohistological staining free-floating sections were washed three times in PBS, fixed in 4% PFA in PBS at room temperature for 2 h, washed in PBS, and permeabilized with 0.5% Triton X-100 (Sigma; catalog no. T9284). Triton X-100 was replaced by the blocking solution (1% NGS in PBS) at room temperature for 1 h, followed by overnight incubation at 4 °C with the primary antibody (anti-Iba1; Wako Labo-

ratories; catalog no. 019-19741) diluted 1:1,000 in PBS or anti-GFAP (G 3893; Sigma) diluted 1:500 in blocking solution. On the next day the antibody was replaced by fresh antibody solution for 16–20 h. Subsequently, the sections were washed three times with PBS and were incubated for 16 h with the secondary antibody, Cy3-conjugated goat anti-rabbit IgG for Iba1 or Cy3-conjugated goat anti-mouse IgG for GFAP (Jackson ImmunoResearch; catalog no. 115-165-003), each diluted 1:600 in PBS at 4 °C. After renewed washing, sections were counterstained with DAPI (diluted 1:1,000 in PBS), washed, and coverslipped with NPG. Sections were examined with a Nikon A1R MP confocal microscope, and z-stacks were generated. Different channels were merged with the Image J 1.46r software (National Institutes of Health). A protocol modified from Chatterjee et al. (54) was used for generating organotypic slice cultures. Organotypic slices were checked for their viability according to Connelly et al. (55).

Statistics. Data are presented as means ± SEM. Statistical analyses were performed using GraphPad Prism 6 for Windows, version 6.01 (GraphPad Software Inc.). Score data were analyzed using the unpaired Mann–Whitney test. For all other analyses the two-tailed, unpaired Student's t test was used. For

calculation of extended disease parameters (*SI Appendix*, Table S2) Fisher's exact test was used.

1. Trapp BD, Nave KA (2008) Multiple sclerosis: An immune or neurodegenerative disorder? *Annu Rev Neurosci* 31:247–269.
2. Trapp BD, et al. (1998) Axonal transection in the lesions of multiple sclerosis. *N Engl J Med* 338:278–285.
3. Brownlee WJ, Hardy TA, Fazekas F, Miller DH (November 23, 2016) Diagnosis of multiple sclerosis: Progress and challenges. *Lancet*, 10.1016/S0140-6736(16)30959-X.
4. Comi G, Radaelli M, Soelberg Sorensen P (November 23, 2016) Evolving concepts in the treatment of relapsing multiple sclerosis. *Lancet*, 10.1016/S0140-6736(16)32388-1.
5. Takano Y, et al. (2004) Study of drug effects of calcium channel blockers on retinal degeneration of rd mouse. *Biochem Biophys Res Commun* 313:1015–1022.
6. Li Y, Hu X, Liu Y, Bao Y, An L (2009) Nimodipine protects dopaminergic neurons against inflammation-mediated degeneration through inhibition of microglial activation. *Neuropharmacology* 56:580–589.
7. Levy A, et al. (1991) Nimodipine improves spatial working memory and elevates hippocampal acetylcholine in young rats. *Pharmacol Biochem Behav* 39:781–786.
8. Damaj MI, Martin BR (1993) Calcium agonists and antagonists of the dihydropyridine type: Effect on nicotine-induced antinociception and hypomotility. *Drug Alcohol Depend* 32:73–79.
9. Kumar N, Singh N, Jaggi AS (2012) Anti-stress effects of cilnidipine and nimodipine in immobilization subjected mice. *Physiol Behav* 105:1148–1155.
10. Kusztos RD, Ingram DK, Spangler EL, London ED (1996) Effects of aging and chronic nimodipine on hippocampal binding of [3H]CGS 19755. *Neurobiol Aging* 17:453–457.
11. Taya K, Watanabe Y, Kobayashi H, Fujiwara M (2000) Nimodipine improves the disruption of spatial cognition induced by cerebral ischemia. *Physiol Behav* 70:19–25.
12. de Jong GI, Buwalda B, Schuurman T, Luiten PG (1992) Synaptic plasticity in the dentate gyrus of aged rats is altered after chronic nimodipine application. *Brain Res* 596:345–348.
13. Singh A, Verma P, Balaji G, Samantaray S, Mohanakumar KP (2016) Nimodipine, an L-type calcium channel blocker attenuates mitochondrial dysfunctions to protect against 1-methyl-4-phenyl-1,2,3,6-tetrahydropyridine-induced Parkinsonism in mice. *Neurochem Int* 99:221–232.
14. Lassmann H (2003) Axonal injury in multiple sclerosis. *J Neurol Neurosurg Psychiatry* 74:695–697.
15. Stromnes IM, Goverman JM (2006) Active induction of experimental allergic encephalomyelitis. *Nat Protoc* 1:1810–1819.
16. Kuerten S, et al. (2011) Myelin-reactive antibodies mediate the pathology of MBP-PLP fusion protein MP4-induced EAE. *Clin Immunol* 140:54–62.
17. Bishnoi M, Chopra K, Kulkarni SK (2008) Protective effect of L-type calcium channel blockers against haloperidol-induced orofacial dyskinesia: A behavioural, biochemical and neurochemical study. *Neurochem Res* 33:1869–1880.
18. Pileblad E, Carlsson A (1986) In vivo effects of the Ca2+-antagonist nimodipine on dopamine metabolism in mouse brain. *J Neural Transm* 66:171–187.
19. Guy J, Ellis EA, Hope GM, Emerson S (1991) Maintenance of myelinated fibre g ratio in acute experimental allergic encephalomyelitis. *Brain* 114:281–294.
20. Recks MS, et al. (2013) Early axonal damage and progressive myelin pathology define the kinetics of CNS histopathology in a mouse model of multiple sclerosis. *Clin Immunol* 149:32–45.
21. Lang J, et al. (2013) Adenomatous polyposis coli regulates oligodendroglial development. *J Neurosci* 33(7):3113–3130.
22. Henn A, et al. (2009) The suitability of BV2 cells as alternative model system for primary microglia cultures or for animal experiments examining brain inflammation. *ALTEX* 26:83–94.
23. Stansley B, Post J, Hensley K (2012) A comparative review of cell culture systems for the study of microglial biology in Alzheimer's disease. *J Neuroinflammation* 9:115.
24. Furukawa T, et al. (1999) Selectivities of dihydropyridine derivatives in blocking Ca(2+) channel subtypes expressed in Xenopus oocytes. *J Pharmacol Exp Ther* 291:464–473.
25. Brewer LD, et al. (2007) Increased vulnerability of hippocampal neurons with age in culture: Temporal association with increases in NMDA receptor current, NR2A subunit expression and recruitment of L-type calcium channels. *Brain Res* 1151:20–31.
26. Grissmer S, et al. (1994) Pharmacological characterization of five cloned voltage-gated K+ channels, types Kv1.1, 1.2, 1.3, 1.5, and 3.1, stably expressed in mammalian cell lines. *Mol Pharmacol* 45:1227–1234.
27. Wulff H, Castle NA, Pardo LA (2009) Voltage-gated potassium channels as therapeutic targets. *Nat Rev Drug Discov* 8:982–1001.
28. Choi BY, et al. (2015) Inhibition of NADPH oxidase activation reduces EAE-induced white matter damage in mice. *J Neuroinflammation* 12:104.
29. Gonsette RE (2008) Oxidative stress and excitotoxicity: A therapeutic issue in multiple sclerosis? *Mult Scler* 14:22–34.
30. Livak KJ, Schmittgen TD (2001) Analysis of relative gene expression data using real-time quantitative PCR and the 2(-Delta Delta C(T)) Method. *Methods* 25:402–408.
31. Rottlaender A, Kuerten S (2015) Neuroprotection in multiple sclerosis (MS) research. *Int J Mol Sci* 16:14850–14865.
32. Tekkök SB, Goldberg MP (2001) Ampa/kainate receptor activation mediates hypoxic oligodendrocyte death and axonal injury in cerebral white matter. *J Neurosci* 21:4237–4248.
33. Chandy KG, DeCoursey TE, Cahalan MD, McLaughlin C, Gupta S (1984) Voltage-gated potassium channels are required for human T lymphocyte activation. *J Exp Med* 160:369–385.
34. Wulff H, Kolski-Andreaco A, Sankaranarayanan A, Sabatier JM, Shakkottai V (2007) Modulators of small- and intermediate-conductance calcium-activated potassium channels and their therapeutic indications. *Curr Med Chem* 14:1437–1457.
35. Färber K, Kettenmann H (2005) Physiology of microglial cells. *Brain Res Brain Res Rev* 48:133–143.
36. Shen XZ, et al. (2015) Microglia participate in neurogenic regulation of hypertension. *Hypertension* 66:309–316.
37. Pradhan VD, Das S, Surve P, Ghosh K (2012) Toll-like receptors in autoimmunity with special reference to systemic lupus erythematosus. *Indian J Hum Genet* 18:155–160.
38. Moon JS, et al. (2016) NOX4-dependent fatty acid oxidation promotes NLRP3 inflammasome activation in macrophages. *Nat Med* 22:1002–1012.
39. Stadelmann C, Wegner C, Brück W (2011) Inflammation, demyelination, and degeneration - recent insights from MS pathology. *Biochim Biophys Acta* 1812:275–282.
40. Giovannoni G, Heales SJ, Land JM, Thompson EJ (1998) The potential role of nitric oxide in multiple sclerosis. *Mult Scler* 4:212–216.
41. Hobbs AJ, Higgs A, Moncada S (1999) Inhibition of nitric oxide synthase as a potential therapeutic target. *Annu Rev Pharmacol Toxicol* 39:191–220.
42. Hauser SL, Chan JR, Oksenberg JR (2013) Multiple sclerosis: Prospects and promise. *Ann Neurol* 74:317–327.
43. Franklin RJM, ffrench-Constant C, Edgar JM, Smith KJ (2012) Neuroprotection and repair in multiple sclerosis. *Nat Rev Neurol* 8:624–634.
44. Waxman SG (2006) Axonal conduction and injury in multiple sclerosis: The role of sodium channels. *Nat Rev Neurosci* 7:932–941.
45. Craner MJ, et al. (2005) Sodium channels contribute to microglia/macrophage activation and function in EAE and MS. *Glia* 49:220–229.
46. Dulamea A (2015) Mesenchymal stem cells in multiple sclerosis - translation to clinical trials. *J Med Life* 8:24–27.
47. Kettenmann H, Hanisch U-K, Noda M, Verkhratsky A (2011) Physiology of microglia. *Physiol Rev* 91:461–553.
48. Nair A, Frederick TJ, Miller SD (2008) Astrocytes in multiple sclerosis: A product of their environment. *Cell Mol Life Sci* 65:2702–2720.
49. National Research Council (2011) *Guide for the Care and Use of Laboratory Animals* (National Academies Press, Washington, DC), 8th Ed.
50. Shen AN, Cummings C, Pope D, Hoffman D, Newland MC (2016) A bout analysis reveals age-related methylmercury neurotoxicity and nimodipine neuroprotection. *Behav Brain Res* 311:147–159.
51. Herzfeld E, et al. (2014) Investigation of the neuroprotective impact of nimodipine on Neuro2a cells by means of a surgery-like stress model. *Int J Mol Sci* 15:18453–18465.
52. Wang H, et al. (2014) pH-sensitive NMDA inhibitors improve outcome in a murine model of SAH. *Neurocrit Care* 20:119–131.
53. Kendziorski CM, Newton MA, Lan H, Gould MN (2003) On parametric empirical Bayes methods for comparing multiple groups using replicated gene expression profiles. *Stat Med* 22(24):3899–3914.
54. Chatterjee D, Biswas K, Nag S, Ramachandra SG, Das Sarma J (2013) Microglia play a major role in direct viral-induced demyelination. *Clin Dev Immunol* 2013:510396.
55. Connelly CA, Chen LC, Colquhoun SD (2000) Metabolic activity of cultured rat brainstem, hippocampal and spinal cord slices. *J Neurosci Methods* 99:1–7.